Transonic Time Responses of the MBB A-3 Supercritical Airfoil Including Active Controls

J. T. Batina* and T. Y. Yang†
Purdue University, West Lafayette, Indiana

Aeroelastic time-response analyses are performed for the MBB A-3 supercritical airfoil in small-disturbance transonic flow based on the use of transonic code LTRAN2-NLR. Three degrees of freedom are considered: plunge, pitch, and aileron pitch. The main objective was to investigate the applicability and accuracy of state-space aeroelastic modeling for two-dimensional airfoils with active controls in transonic flow. A state-space aeroelastic model was formulated using a Padé aerodynamic approximation. The resulting equations are explicitly solved in the time domain yielding the aeroelastic displacement responses. Parallel time-marching response histories were determined numerically through a coupled integration of the structural equations of motion with the unsteady aerodynamic forces of LTRAN2-NLR. The Padé and time-integration responses are in good agreement. The Padé eigenvalues compare well with the time-marching damping and frequency estimates. A simple feedback control loop was included in the aeroelastic system to study the effects of active control on the aeroelastic response. A variety of control laws utilizing displacement, velocity, and acceleration sensing were considered. Transonic time-response behavior of the MBB A-3 airfoil is discussed and comparisons are made.

Nomenclature

a_h = nondimensional elastic axis location, positive aft of midchord
b,c = airfoil semichord and chord, respectively
c_ℓ = steady lift coefficient
c_β = nondimensional aileron hinge line location
C_p, C_p^* = pressure coefficient; critical pressure coefficient
$[C]$ = nondimensional damping matrix
$\{G\}$ = control distribution vector
h = plunging degree of freedom, positive downward from elastic axis
K_A, K_D, K_V = acceleration, displacement, and velocity control gains, respectively
$[K]$ = nondimensional stiffness matrix
m = mass of the airfoil per unit span
M = freestream Mach number
$[M]$ = nondimensional mass matrix
p = nondimensional sensor location, positive aft of midchord
$\{p\}$ = aerodynamic load vector
r_α, r_β = radii of gyration of airfoil about elastic axis and of aileron about hinge axis, respectively
s = $\sigma + i\omega$, Laplace transform variable
$t,\bar{t}$ = time; $\omega_\alpha t$, nondimensional time
U, U^* = freestream velocity; $U/b\omega_\alpha$, nondimensional flight speed
U_D, U_D^* = divergence speed; $U_D/b\omega_\alpha$, nondimensional divergence speed
U_F, U_F^* = flutter speed; $U_F/b\omega_\alpha$, nondimensional flutter speed
x_α, x_β = nondimensional distances from elastic axis to airfoil mass center and hinge line to aileron mass center, respectively
$\{X\}, \{Z\}$ = displacement and state vectors, respectively
α = airfoil pitching degree of freedom, positive leading edge up
α_0 = mean angle of attack, positive leading edge up
β = aileron pitching degree of freedom, positive trailing edge down
β_c = control surface command rotation
ζ_β = control surface viscous damping ratio
μ = $m/\pi\rho b^2$, airfoil mass ratio
ξ = h/b, nondimensional plunging degree of freedom, positive downward from elastic axis
ξ_s = nondimensional sensor plunging displacement
ρ = freestream air density
$\omega_h, \omega_\alpha, \omega_\beta$ = uncoupled natural frequencies of plunging; pitching about elastic axis, and aileron pitching about hinge axis, respectively

Received March 2, 1984; presented as Paper 84-0873 at the AIAA/ASME/ASCE/AHS 25th Structures, Structural Dynamics and Materials Conference, Palm Springs, Calif., May 14-16, 1984; revision received Jan. 8, 1985.

*David Ross Fellow, School of Aeronautics and Astronautics (presently, Aerospace Engineer, Loads and Aeroelasticity Division, Unsteady Aerodynamics Branch, NASA Langley Research Center, Hampton, Va.). Member AIAA.

†Professor and Dean, Schools of Engineering. Associate Fellow AIAA.

Introduction

AEROELASTIC time-response characteristics of airfoils and wings in small-disturbance transonic flow have recently attracted considerable research interest. In the time-response analysis, the structural equations of motion are coupled to transonic aerodynamic codes using a numerical integration procedure.

Ballhaus and Goorjian[1] first reported a time-response analysis of a NACA 64A006 airfoil oscillating with a single pitching degree of freedom (dof) at $M = 0.88$. The structural equation of motion was simultaneously integrated in time with the unsteady aerodynamics of their LTRAN2 code.[2]

Rizzetta[3] performed time-response analyses for the NACA 64A010 airfoil oscillating with a single pitching dof and with three dof's: plunge, pitch, and aileron pitch. An Adams-Moulton structural integrator was coupled with the LTRAN2 code to obtain the aeroelastic responses. Significant nonlinear effects were demonstrated using relatively large initial conditions.

Guruswamy and Yang[4] used LTRAN2 to perform time-response analyses for a flat plate and NACA 64A006 airfoil at $M = 0.7$ and 0.85, respectively, with two dof's: plunge and

pitch. A direct integration method based on a linear variation of acceleration was employed to find the time-history dynamic responses of the aeroelastic system. Flutter speeds selected from the separate flutter analysis indeed resulted in neutrally stable time responses.

Borland and Rizzetta[5] used the XTRAN3S code and a centered difference structural integration technique for the time response of three-dimensional wings in transonic flow. A flutter boundary for a rectangular wing of parabolic arc cross section was determined by computing displacement response histories at different values of freestream dynamic pressure.

Yang and Chen[6] and Yang and Batina[7] presented three dof time-response results for the NACA 64A006, NACA 64A010, and MBB A-3 airfoils. The structural integrator with the assumed linear variation of acceleration was coupled to the LTRAN2-NLR[8] and USTS[9] transonic codes. Flight speeds used to obtain neutrally stable time responses were shown to be equal or very close to the flutter speeds determined in separate flutter analyses.

Edwards et al.[10] presented transonic flutter boundaries for two dof NACA 64A010 and MBB A-3 airfoils determined by time-response calculations and a modal identification technique. Seven alternative integration methods were examined and evaluated. The preferred algorithm was a modified state transition matrix integrator. A state-space aeroelastic model employing Padé approximants demonstrated the accuracy of the time-marching analysis for subcritical, critical, and supercritical flutter conditions.

In the present research, transonic time-response calculations are performed using LTRAN2-NLR for two conventional airfoils (NACA 64A006 and NACA 64A010) and one supercritical airfoil (MBB A-3).[11] Only representative results for the MBB A-3 airfoil are presented here. Three dof's—plunge, pitch, and aileron pitch—are considered. The objectives for the present time-response analyses are: 1) to investigate the applicability and accuracy of state-space aeroelastic modeling for two-dimensional airfoils with active controls in transonic flow; 2) to study the response behavior of the subject airfoils with the inclusion of active controls for flutter suppression; and 3) to gain further insight into the three dof response histories when the forced motion starting conditions of Refs. 6 and 7 are eliminated.

A state-space aeroelastic model, termed the Padé model, was formulated using generalized aerodynamic forces approximated by an interpolating function in the variable s. This Padé model results in a set of linear, first-order, constant-coefficient differential equations. In Ref. 12 these equations were solved in the Laplace domain with the resulting eigenvalues plotted in a "root-locus" type of format. Alternatively in the present study, the Padé model is solved explicitly in the time domain, with appropriate initial conditions, yielding the aeroelastic time-response histories. As verification of the Padé results, parallel time-marching response calculations are carried out by simultaneously integrating the structural equations of motion along with the unsteady aerodynamic forces of transonic code LTRAN2-NLR. Comparisons are made between the Padé model displacement responses and the time-integration results. A modal identification technique is used to estimate the damping and frequency of the aeroelastic modes from the time-marching response curves. Padé model eigenvalues are directly compared with these time-marching modal estimates in the complex s plane. A simple, constant-gain feedback control law is included in the aeroelastic system to assess the accuracy of the Padé model for active controls applications as well as to study the effects of active control on the aeroelastic response. The control equations are intentionally simple for illustrative purposes. A variety of control laws utilizing displacement, velocity, and acceleration sensing are considered. Transonic time-response behavior of the MBB A-3 airfoil is discussed and comparisons between Padé model and time-marching results are made.

Padé Model

The aeroelastic equations of motion for a typical airfoil section oscillating with three dof's can be written as[12-14]

$$[M]\{\ddot{X}\} + [C]\{\dot{X}\} + [K]\{X\} = \{p\} + \{G\}\beta_c \qquad (1)$$

where $\{X\} = [\xi \ \alpha \ \beta]^T$ is the displacement vector containing plunge displacement ξ, pitching rotation α, and aileron pitching rotation β.

A Padé model was formulated in Ref. 12 using linear superposition of airloads and approximating the aerodynamic forces by an interpolating function in the variable s. These generalized aerodynamic forces were then available as linear differential equations which, when coupled to Eq. (1), lead to a first-order matrix equation

$$\{\dot{Z}\} = [A]\{Z\} + \{B\}\beta_c \qquad (2)$$

where $\{Z\}$ contains the displacements, velocities, and augmented states.

For closed-loop study, a simple, constant-gain, partial feedback control law has been assumed of the form

$$\beta_c = K_D\xi_s + K_V\dot{\xi}_s + K_A\ddot{\xi}_s \qquad (3)$$

where K_D, K_V, and K_A are the displacement, velocity, and acceleration control gains, respectively, and ξ_s the sensor-measured plunging motion. A sensor was located along the airfoil chord a distance pb $(-1.0<p<c_\beta)$ aft of midchord. An indication of plunging ξ and pitching α motions is thus obtained since

$$\xi_s = \lfloor H \rfloor \{X\} \qquad (4)$$

where $[H] = [1.0\ (p-a_h)\ 0.0]$. Following Ref. 12, the sensor was placed forward of the control surface hinge line at 70% chord ($p=0.4$). The control system is implemented for closed-loop analyses by including the control law [Eq. (3)] expressed in terms of the state vector $\{Z\}$ in the Padé model. The equations are then of the form

$$\{\dot{Z}\} = [A]\{Z\} \qquad (5)$$

which may be solved in either the Laplace or time domains.

Laplace Domain Solution

The Laplace domain solution of the Padé model yields the eigenvalues (and corresponding eigenvectors) of the aeroelastic system. Of primary interest are the complex conjugate eigenvalues of the structural dof's.

The Padé model is solved by reducing Eq. (5) to an eigenvalue problem

$$\lambda_j\{Z\}_j = [A]\{Z\}_j \qquad (6)$$

where $\lambda_j = (s/\omega_\alpha)_j$ is an eigenvalue and $\{Z\}_j$ the corresponding eigenvector. Equation (6) is easily solved using standard eigenvalue solution techniques since $[A]$ is a real constant matrix. Results may be presented in a root-locus format.

In addition to the complex conjugate poles of the structural dof's, additional eigenvalues are determined that correspond to the augmented states. These eigenvalues usually lie on or very close to the negative real axis in the complex s plane.

Time-Domain Solution

The explicit time-domain solution of the Padé model yields the aeroelastic time responses for the state vector $\{Z(\bar{t})\}$. This analysis requires a priori knowledge of the eigenvalues and eigenvectors of the matrix $[A]$. Of primary interest are the responses of the structural dof's.

The solution of a set of first-order, constant-coefficient differential equations is given in common textbooks on linear analysis such as Ref. 15. In matrix form, the solution to Eq. (5) may be written as

$$\{Z(\bar{t})\} = [P][L][P]^{-1}\{Z_0\} \tag{7}$$

where $[L]$ is a diagonal matrix with diagonal elements $e^{\lambda_j \bar{t}}$, λ_j the eigenvalues of $[A]$, $[P]$ a square matrix whose columns are the corresponding eigenvectors of $[A]$, and $\{Z_0\} = \{Z(0)\}$ the vector of appropriate initial conditions.

Defining $x_1 = \xi$, $x_2 = \alpha$, and $x_3 = \beta$, expanding the right-hand side of Eq. (7), and taking real parts, the Padé model displacement responses are

$$x_i(\bar{t}) = Re \sum_{j=1}^{n} (y_o)_j P_j^i e^{\lambda_j \bar{t}}, \qquad i = 1,2,3 \tag{8}$$

where $(y_0)_j$ is an element of $\{Y_0\} = [P]^{-1}\{Z_0\}$ and P_j^i the i^{th} element of the j^{th} column (eigenvector) of $[P]$.

As discussed by Edwards et al.,[16] the exact aeroelastic response is made up of two parts

$$x_i(\bar{t}) = x_{i_r}(\bar{t}) + x_{i_{nr}}(\bar{t}) \tag{9}$$

where $x_{i_r}(\bar{t})$ and $x_{i_{nr}}(\bar{t})$ are the "rational" and "nonrational" portions, respectively. The rational part is due to the isolated poles introduced by the structural dof's; the nonrational part comes from an integration along a branch cut on the negative real axis of the complex s plane. Oscillatory response motions characteristic of flutter are due entirely to the rational part $x_{i_r}(\bar{t})$, whereas the response of the nonrational part $x_{i_{nr}}(\bar{t})$ is nonoscillatory and decays monotonically to zero. Therefore, the terms in Eq. (8) due to the structural dof's may be identified as the rational portion of the aeroelastic response; the terms in Eq. (8) due to the discrete aerodynamic poles along the negative real axis corresponding to the augmented states are an estimate of the nonrational portion. Thus, the time-domain solution of the Padé model approximates the total response of the aeroelastic system.

Time-Marching Aeroelastic Solution

The time-marching solution determines the aeroelastic responses by simultaneously integrating the structural equations of motion along with the unsteady aerodynamic forces of transonic code LTRAN2-NLR. In this analysis, neither the linear superposition of airloads nor the Padé aerodynamic approximation are needed.

Equations of Motion for Time Integration

By expressing the control law [Eq. (3)] in terms of the airfoil motion as

$$\beta_c = K_D \lfloor H \rfloor \{X\} + K_V \lfloor H \rfloor \{\dot{X}\} + K_A \lfloor H \rfloor \{\ddot{X}\} \tag{10}$$

the aeroelastic equations of motion [Eq. (1)] may be written in general form for time integration as

$$[M^*]\{\ddot{X}\} + [C^*]\{\dot{X}\} + [K^*]\{X\} = \{p\} \tag{11}$$

where

$$[M^*] = [M] - K_A\{G\}\lfloor H \rfloor \tag{12a}$$

$$[C^*] = [C] - K_V\{G\}\lfloor H \rfloor \tag{12b}$$

$$[K^*] = [K] - K_D\{G\}\lfloor H \rfloor \tag{12c}$$

Equation (11) is numerically integrated using the modified state-transition matrix integrator of Edwards et al.[10] to find the time-history dynamic responses of the aeroelastic system. Details of the response solution procedure are given in Ref. 10. The time-step size selected corresponds to approximately 120 time steps per cycle of oscillatory motion due to the bending mode.

Modal Identification of Time-Marching Response

A modal identification technique is used to determine the damping, frequency, amplitude, and phase of the aeroelastic modes from the time-marching displacement response histories. A method similar to that of Bennett and Desmarais[17] was used to curve fit the time responses by complex exponential functions (damped cosine and sine waves) of the form

$$x_i(\bar{t}) = a_0 + \sum_{j=1}^{m} e^{(\sigma/\omega_\alpha)_j \bar{t}} \left[a_j \cos\left(\frac{\omega}{\omega_\alpha}\right)_j \bar{t} + b_j \sin\left(\frac{\omega}{\omega_\alpha}\right)_j \bar{t} \right] \tag{13}$$

The damping and frequency of the complex modes thus obtained

$$\left(\frac{\sigma}{\omega_\alpha}\right)_j \pm i\left(\frac{\omega}{\omega_\alpha}\right)_j = \left(\frac{s}{\omega_\alpha}\right)_j = \lambda_j \tag{14}$$

are estimates of the aeroelastic eigenvalues and may then be directly compared with those computed by the Laplace domain solution of the Padé model.

Results and Discussion

Transonic aeroelastic time-response analyses were performed for three airfoil configurations[11] (NACA 64A006, NACA 64A010, and MBB A-3) based on the use of the transonic code LTRAN2-NLR. Representative results are presented here for the MBB A-3 supercritical airfoil only. Time-response behavior of the MBB A-3 airfoil was studied at the design Mach number $M = 0.765$ and at zero mean angle of attack $\alpha_0 = 0$ deg and the design steady lift coefficient $c_\ell = 0.58$. The mean angle of attack necessary to match $c_\ell = 0.58$ using LTRAN2-NLR is $\alpha_0 = 0.86$ deg. The aeroelastic parameter values selected are the same as those used in Ref. 12 and are listed in Table 1. The airfoil has a trailing-edge control surface of 25% chord.

The MBB A-3 steady pressure distribution computed using LTRAN2-NLR at $M = 0.765$ and $c_\ell = 0.58$ is shown in Fig. 1 along with the airfoil contour. These steady pressure data compare well with the experimental results of Bucciantini et al.[18] There is a relatively weak shock wave on the airfoil upper surface near 55-60% chord. Steady pressure distributions for all of the cases considered indicate shock locations in the range of 50-65% chord and shock strengths that are well within the range of applicability of transonic small-disturbance theory.[11]

Open-Loop Response Results

Open-loop stability analyses were performed first to determine the frequency and damping of the aeroelastic modes as a function of flight speed.[12] These calculations were performed using the Padé model solved in the Laplace domain with results plotted in a flight speed root-locus format. As an example, open-loop flight speed root-loci are presented in Fig. 2 for the $c_\ell = 0.58$ case. The bending-dominated root locus becomes the flutter mode at a nondimensional flutter speed U_F^* of 2.370; the divergence speed, where an aerodynamic pole associated with one of the augmented states crosses through

Table 1 Aeroelastic parameter values for time-response analyses

$\omega_h/\omega_\alpha = 0.3$	$c_\beta = 0.5$	$x_\beta = 0.008$
$\omega_\beta/\omega_\alpha = 1.5$	$x_\alpha = 0.2$	$r_\beta = 0.06$
$\mu = 50.0$	$r_\alpha = 0.5$	$\zeta_\beta = 0.0$
$a_h = -0.2$		

Table 2 Summary of open-loop flutter and divergence speeds for the MBB A-3 airfoil

Airfoil	Flutter method	Flutter speed U_F^*	Divergence speed U_D^*	U_D/U_F
MBB A-3 $M=0.765$, $\alpha=0$ deg	Padé	2.588	3.516	1.359
	p-k	2.596		
MBB A-3 $M=0.765$, $c_\ell=0.58$	Padé	2.370	3.320	1.401
	p-k	2.403		
Linear theory $M=0.765$	Padé	2.711	3.611	1.332
	p-k	2.729		

the origin, is $U_D^*=3.320$. A summary containing MBB A-3 flutter and divergence speeds for both $\alpha_0=0$ deg and $c_\ell=0.58$ cases including linear subsonic theory values is given in Table 2. Flutter speeds from a *p-k* method[19] flutter analysis are also tabulated for further comparison.

Alternatively, the Padé model was solved in the time domain for the three dof displacement responses. These time-response histories, computed using Eq. (8), are shown in Fig. 3a for three different values of the flight speed ratio U/U_F. A 1% semichord plunge displacement was used as initial condition. Padé time responses for $U/U_F=1.0$ are exactly neutrally stable after the initial torsion and aileron mode transients die out. Results for $U/U_F=0.844$, corresponding to $U^*=2.0$, show converging oscillatory response behavior (subcritical); results for $U/U_F=1.156$ indicate diverging oscillatory response behavior (supercritical).

Time-marching solutions were then obtained using LTRAN2-NLR for verification of the Padé model results. Response histories of the three dof's are shown in Fig. 3b. The initial conditions and three flight speed ratios U/U_F are the same as those used in the Padé solutions. The nondimensional flutter speed U_F^* used for time-marching analyses was the *p-k* method value. Comparison of the Padé time-domain solutions shown in Fig. 3a with the time-marching solutions shown in Fig. 3b indicates remarkably good agreement.

The time-marching displacement responses were then curve fit using Eq. (13) to determine the damping and frequency of the aeroelastic modes. As shown in Fig. 3b, the plunge displacement response ξ does not contain the higher-frequency torsion and aileron transients in the first two cycles of motion as do the α and β responses. Hence, only the bending mode could be identified from the modal curve fit of the ξ response. From the pitching response α, both the dominant bending mode as well as the higher-frequency torsion mode were identified. From the aileron pitching response β, all three aeroelastic modes (bending, torsion, and aileron) were determined. These damping and frequency values are compared with Padé and *p-k* eigenvalues in Table 3. The five sets of results generally compare well. Agreement in frequency ω/ω_α is, in general, better than that for damping σ/ω_α. Agreement for the lower-frequency bending and torsion modes is, in general, better than that for the higher-frequency aileron mode. These differences may be attributed to the following factors: 1) the Padé and *p-k* eigenvalues are less accurate at higher damping values; 2) the structural integration is performed with only 25-30 time steps per cycle of the aileron mode; and 3) since the aileron mode has more damping in comparison with bending and torsion, its contribution to the responses dies out very quickly, leaving very little information for curve fitting. Modal fits at $U/U_F=1.0$ reveal that the time-marching responses corresponding to flutter are actually very slightly diverging. A graphic comparison between the Padé model eigenvalues and the time-marching modal estimates for the bending and torsion modes is given in Fig. 4. The two sets of results agree well.

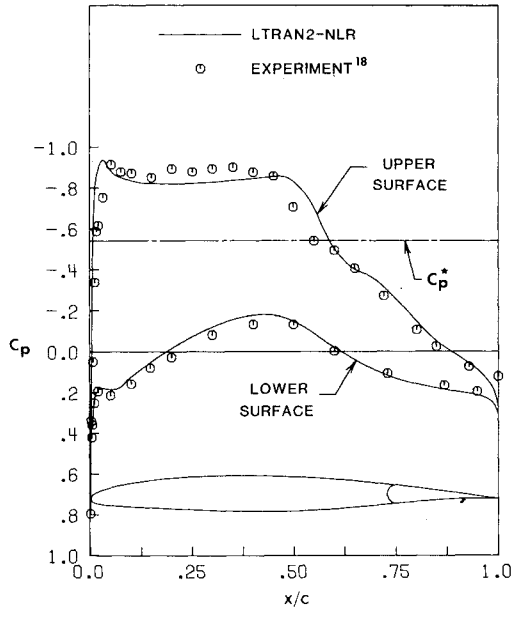

Fig. 1 Steady pressure distributions for the MBB A-3 airfoil at $M=0.765$ and $c_\ell=0.58$.

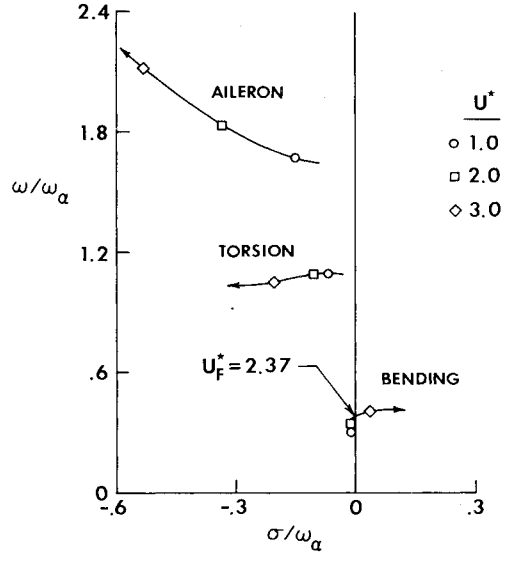

Fig. 2 MBB A-3 open-loop flight speed root loci at $M=0.765$ and $c_\ell=0.58$.

Closed-Loop Response Results

Closed-loop time-response calculations were performed to determine the accuracy of the Padé model with the inclusion of active feedback control. Aeroelastic effects due to single-gain control laws utilizing displacement, velocity, or acceleration sensing were studied by setting two of the three control gains K_D, K_V, and K_A equal to zero. The Padé model calculations were performed first at the flight speed set equal to the open-loop flutter value to determine the effects of active control on the flutter mode. The poles and zeros of the Padé model were determined. Representative control gain root-loci for the NACA 64A010 airfoil at $M=0.8$ and for the MBB A-3 airfoil at $M=0.765$ and $c_\ell=0.58$ were reported in Refs. 12 and 20, respectively.

Effects of Acceleration Feedback

Aeroelastic effects due to acceleration sensing $\ddot{\xi}_s$ on displacement responses were investigated for successive increased acceleration feedback. Values selected for the control

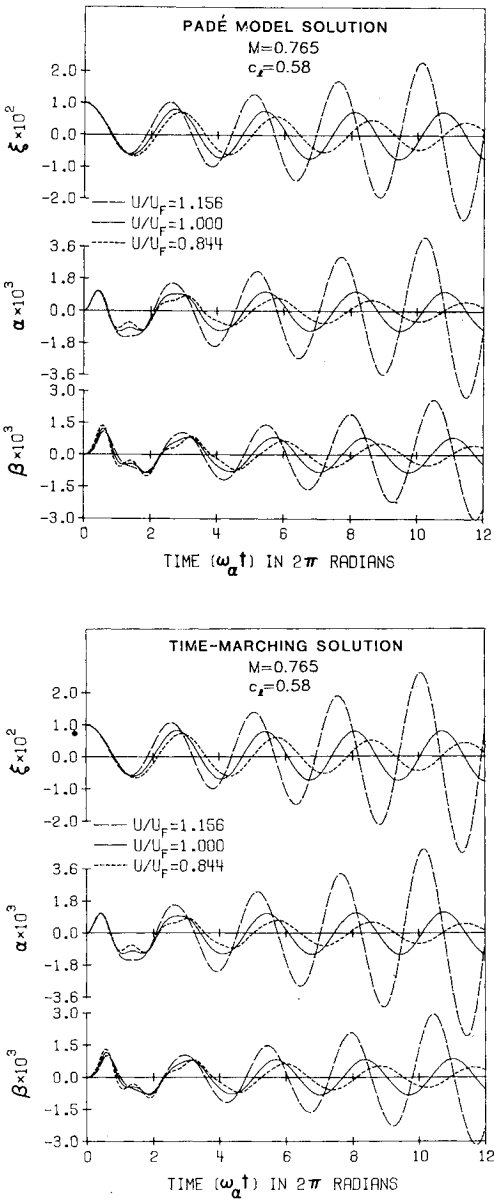

Fig. 3 Effect of flight speed on MBB A-3 open-loop displacement responses at $M=0.765$ and $c_\ell=0.58$. a) Explicit time-domain solution of the Padé model. b) Coupled LTRAN2-NLR time-marching solution.

gains were $K_A=6.0$, 12.0, and 18.0. Padé model and time-marching displacement response histories for the $c_\ell=0.58$ case at $U/U_F=1.0$ are shown in Figs. 5a and 5b, respectively. Padé model response histories resemble the time-marching results very closely. Displacement responses for $c_\ell=0.58$ show consistently increased damping for successively larger acceleration feedback. Also, a higher-frequency transient becomes more visible in the α and β responses for larger values of K_A. This is due to decreased damping of the torsion mode with increasing acceleration feedback. Damping and frequency of the bending and torsion modes determined from the time-marching response histories are compared with the Padé model eigenvalues in Fig. 6. In general, the two sets of results agree well. Agreement in frequency ω/ω_α is generally better than for damping σ/ω_α.

Time-marching responses for the $\alpha_0=0$ deg case at $U/U_F=1.0$ are shown in Fig. 7. Parallel time-domain solutions of the Padé model are very similar to the time-marching curves of Fig. 7 and are therefore not shown here. Time-marching responses for $\alpha_0=0$ deg show that damping is first increased and then decreased for successively larger acceleration gains K_A. Also, there is an increase in the dominant frequency for $K_A=18.0$ shown in the α and β responses. Damping and frequency estimates determined from the time-marching response curves of Fig. 7 are plotted in Fig. 8 along with the Padé model eigenvalues. Again, the two sets of results are in very good agreement.

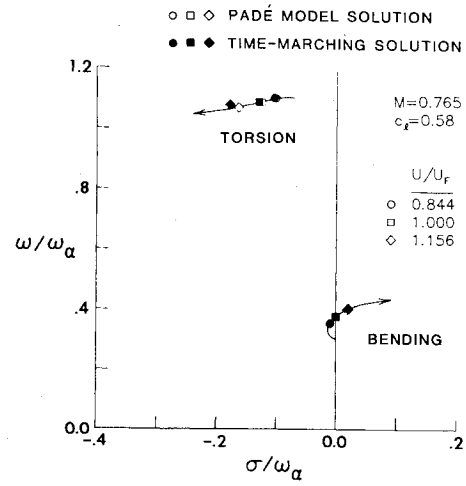

Fig. 4 Comparison between Padé model and time-marching MBB A-3 flight speed root loci for bending and torsion modes at $M=0.765$ and $c_\ell=0.58$.

Table 3 Comparison of Padé and *p-k* eigenvalues with time-marching damping and frequency estimates for the MBB A-3 airfoil at $M=0.765$ and $c_\ell=0.58$

		Bending mode		Torsion mode		Aileron mode	
U/U_F	Method	σ/ω_α	ω/ω_α	σ/ω_α	ω/ω_α	σ/ω_α	ω/ω_α
0.844	Padé	−0.0093	0.3504	−0.1017	1.098	−0.3328	1.829
	p-k	−0.0094	0.3530	−0.1067	1.088	−0.3346	1.871
	ξ response fit	−0.0090	0.3525				
	α response fit	−0.0088	0.3523	−0.1044	1.100		
	β response fit	−0.0088	0.3523	−0.1070	1.101	−0.3145	1.889
1.000	Padé	0.0000	0.3729	−0.1252	1.086	−0.4057	1.923
	p-k	0.0000	0.3757	−0.1324	1.063	−0.4201	1.939
	ξ response fit	0.0010	0.3757				
	α response fit	0.0009	0.3755	−0.1301	1.087		
	β response fit	0.0013	0.3756	−0.1432	1.094	−0.4650	2.139
1.156	Padé	0.0194	0.3977	−0.1643	1.069	−0.4790	2.033
	p-k	0.0177	0.3978	−0.1810	1.019	−0.5094	2.034
	ξ response fit	0.0216	0.4004				
	α response fit	0.0214	0.4001	−0.1785	1.079		
	β response fit	0.0214	0.4003	−0.1964	1.065	−0.6330	2.302

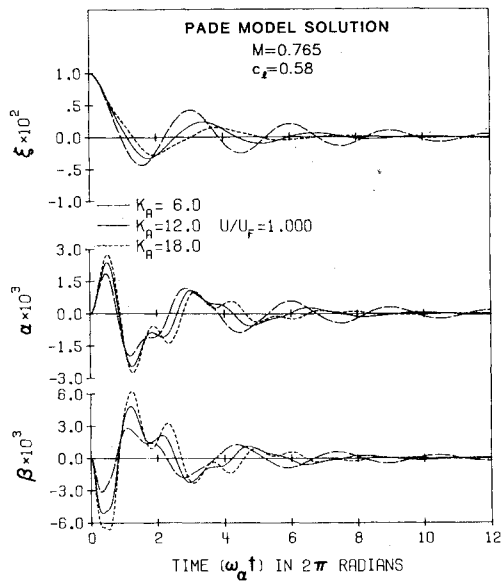

a)

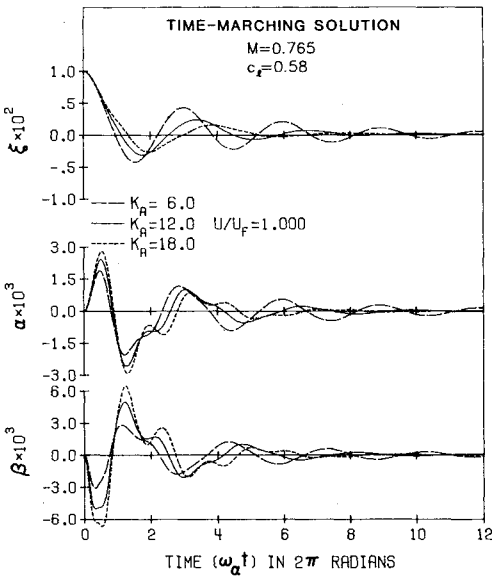

b)

Fig. 5 Effect of acceleration feedback on MBB A-3 displacement responses at the open-loop flutter speed ($U/U_F = 1.0$), $M = 0.765$ and $c_\ell = 0.58$. a) Explicit time-domain solution of the Padé model. b) Coupled LTRAN2-NLR time-marching solution.

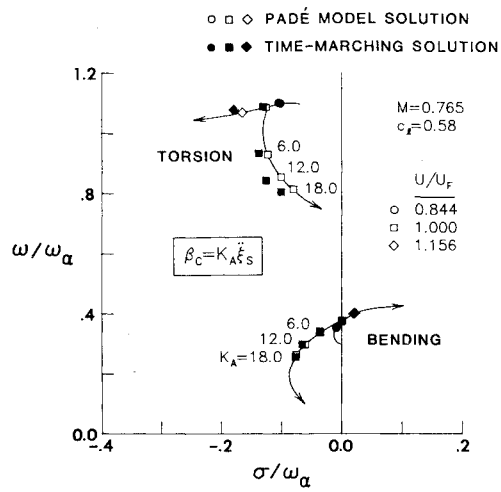

Fig. 6 Effect of acceleration feedback on MBB A-3 bending and torsion modes at the open-loop flutter speed ($U/U_F = 1.0$), $M = 0.765$, and $c_\ell = 0.58$.

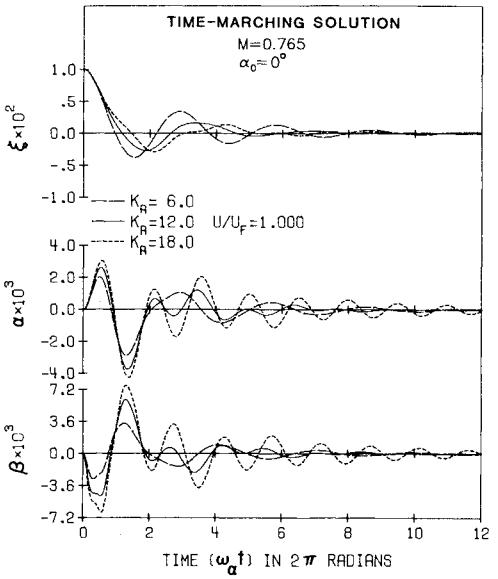

Fig. 7 Effect of acceleration feedback on MBB A-3 time-marching displacement responses at the open-loop flutter speed ($U/U_F = 1.0$), $M = 0.765$, and $\alpha_0 = 0$ deg.

Aeroelastic effects due to acceleration feedback were further investigated using the Padé model.[11,12] Acceleration feedback with $K_A = 12.0$, for example, increased damping in the bending-dominated mode, resulting in flutter speed increases of approximately 19 and 23% for the $\alpha_0 = 0$ deg and $c_\ell = 0.58$ cases, respectively.

Effects of Velocity Feedback

Aeroelastic effects due to velocity sensing $\dot{\xi}_s$ on displacement responses were investigated for successively increased velocity feedback. Values selected for the control gains were $K_V = 3.0$, 6.0, and 9.0. Padé model and time-marching displacement response histories for the $c_\ell = 0.58$ case at $U/U_F = 1.266$ are shown in Figs. 9a and 9b, respectively. The Padé model responses of Fig. 9a are virtually identical to the time-marching responses of Fig. 9b. The three dof displacement responses are bending dominated and converging for all three values of the control gain K_V. As K_V is increased, the response histories become more stable, indicating an increase in bending mode damping at approximately the same frequency. Velocity feedback with positive control gains also sig-

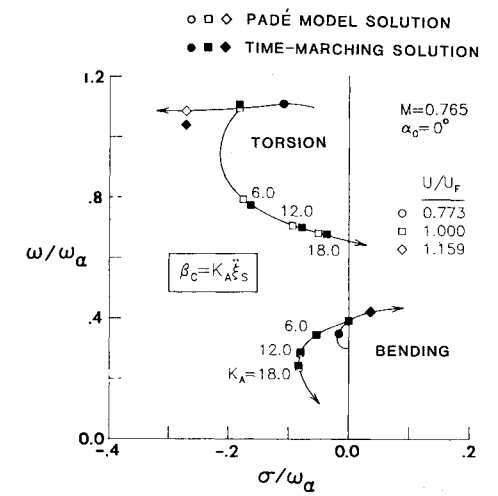

Fig. 8 Effect of acceleration feedback on MBB A-3 bending and torsion modes at the open-loop flutter speed ($U/U_F = 1.0$), $M = 0.765$, and $\alpha_0 = 0$ deg.

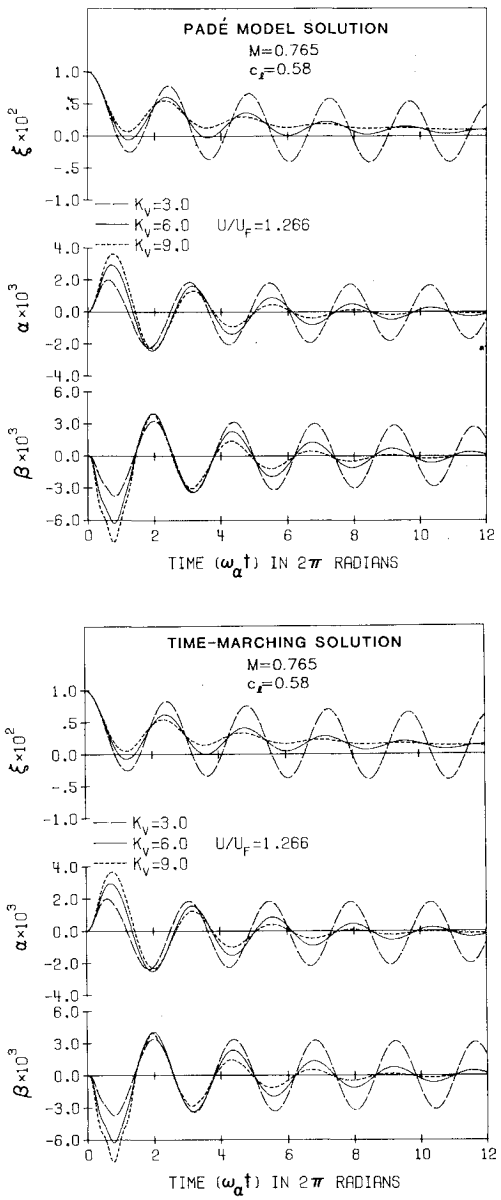

Fig. 9 Effect of velocity feedback on MBB displacement responses at $U/U_F = 1.266$, $M = 0.765$ and $c_\ell = 0.58$. a) Explicit time-domain solution of the Padé model. b) Coupled LTRAN2-NLR time-marching solution.

nificantly increased the nonrational part of the plunge displacement responses as shown in both Figs. 9a and 9b. Here, the plunge transients oscillate about an asymptotically decaying rather than a zero mean value.

Aeroelastic effects due to velocity feedback were further investigated using the Padé model.[11,12] Representative flight speed root loci at $K_V = 6.0$, for example, are shown in Fig. 10 for the $\alpha_0 = 0$ deg and $c_\ell = 0.58$ cases. Closed-loop flight speed root loci for both cases indicate that the damping is significantly increased in torsion and is decreased in the aileron mode. At zero mean angle of attack $\alpha_0 = 0$ deg, the stability of the bending-dominated flutter mode is improved, thus increasing the flutter speed by approximately 12%. At the design condition $c_\ell = 0.58$, the velocity feedback eliminated flutter, completely stabilizing the bending branch. Here, the aeroelastic instability is static divergence at the uncontrolled divergence speed $U_D^* = 3.320$, 40% greater than the open-loop flutter speed.

Effects of Displacement Feedback

Aeroelastic effects due to displacement sensing ξ_s were studied by obtaining time-marching response histories for

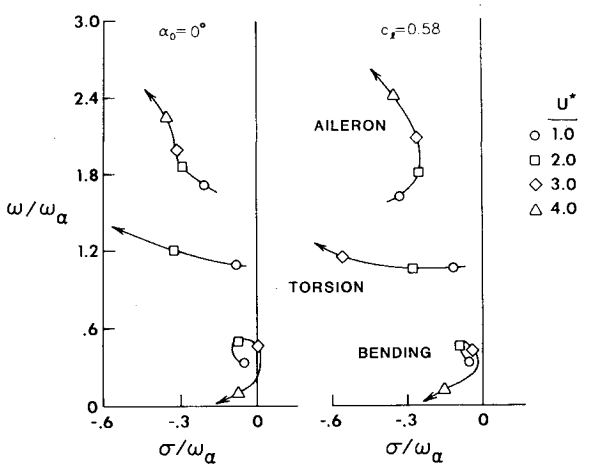

Fig. 10 MBB A-3 velocity feedback ($K_V = 6.0$) flight speed root loci at $M = 0.765$.

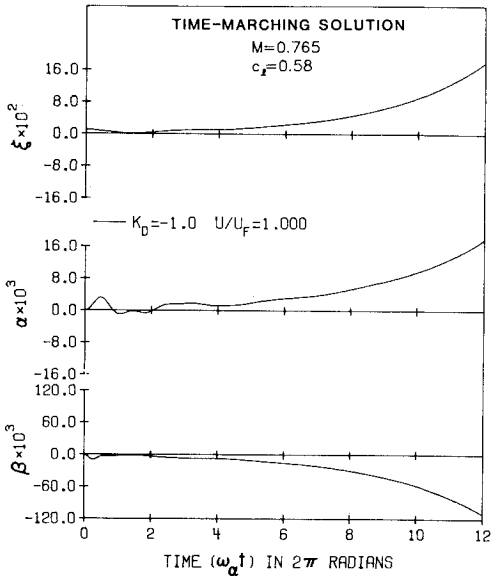

Fig. 11 Effect of displacement feedback on MBB A-3 time-marching displacement responses at the open-loop flutter speed ($U/U_F = 1.0$), $M = 0.765$, and $c_\ell = 0.58$.

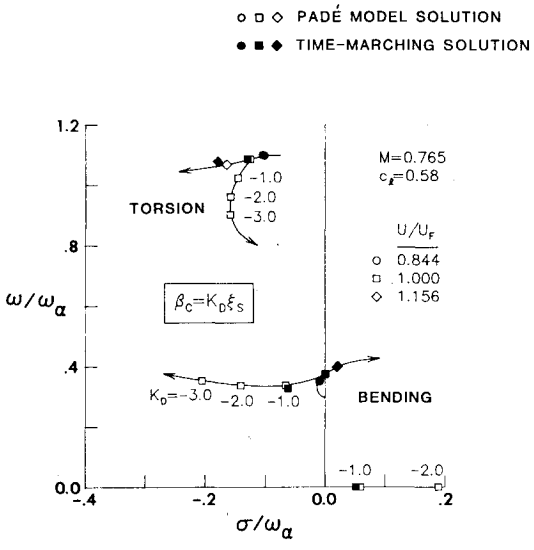

Fig. 12 Effect of displacement feedback on MBB A-3 bending and torsion modes at the open-loop flutter speed ($U/U_F = 1.0$), $M = 0.765$, and $c_\ell = 0.58$.

$K_D = -1.0$ and more detailed Padé model s-plane results. It was shown in Ref. 12 that displacement feedback with negative control gains, for the aeroelastic parameter values assumed here, suppresses flutter but causes static divergence to occur. For the MBB A-3 airfoil at $M = 0.765$, this static divergence occurs for displacement gains $K_D \lesssim -0.6$ for α_0 deg and $K_D \lesssim -0.5$ for $c_\ell = 0.58$. For verification, time-marching responses were obtained for the $c_\ell = 0.58$ case at $U/U_F = 1.0$ and $K_D = -1.0$. These response histories, which are shown in Fig. 11, indicate that flutter has been suppressed and that the displacements are indeed divergent. Comparisons of the Padé model eigenvalues with the limited time-marching damping and frequency estimates are given in Fig. 12. Good agreement is found in predicting this aeroelastic divergence. In addition, displacement feedback with negative control gains increased the damping in bending and decreased the torsion mode frequency. The lower-frequency bending mode damping and frequency values for $K_D = -1.0$ compare well; results from the time-marching modal fits for the higher-frequency torsion and aileron modes were not reliably determined.

Concluding Remarks

Transonic aeroelastic time-response analyses were performed for the MBB A-3 supercritical airfoil based on the use of transonic code LTRAN2-NLR. A state-space aeroelastic model was formulated using generalized aerodynamic forces approximated by a Padé interpolating function. Harmonic transonic aerodynamic data required by this analysis were calculated using LTRAN2-NLR. The Padé model was solved in the Laplace domain with the resulting eigenvalues plotted in flight speed or control gain root-locus format. Alternatively, the Padé model was explicitly solved in the time domain, with appropriate initial conditions, yielding the displacement responses of the three degrees-of-freedom aeroelastic system. Parallel time-marching responses were obtained by simultaneously integrating the structural equations of motion along with the unsteady aerodynamic forces of LTRAN2-NLR. The Padé model and time-marching response histories are in good agreement, thus demonstrating the ability of the Padé equations to model the aeroelastic system accurately. A modal identification technique was applied to the time-marching displacement response curves to estimate the damping and frequency of the aeroelastic modes. Padé model eigenvalues agreed well with these time-marching modal estimates.

Open-loop displacement responses were obtained using both the Padé model and time-marching analyses. Three different flight speeds were considered to investigate subcritical, critical, and supercritical flutter conditions. Good agreement was found between the two sets of aeroelastic response results. Closed-loop displacement responses were obtained using both the Padé model and time-marching analyses. Effects due to a variety of control gains were investigated by adding a simple, constant-gain feedback loop to the aeroelastic equations of motion. The control system and equations were intentionally simple for illustrative purposes. Again, the two sets of aeroelastic response results compared well. Therefore, locally linear state-space aeroelastic modeling was found to be applicable to two-dimensional airfoils with active controls in small-disturbance transonic flow.

Acceleration feedback with positive control gains increased the damping of the bending-dominated responses and raised flutter speeds. Velocity feedback with positive control gains also increased the damping of the bending-dominated displacement responses and alleviated the flutter instability. Also, velocity feedback significantly increased the nonrational portion of the plunge displacement responses. Here, the plunge transients oscillated about an asymptotically decaying rather than a zero mean value. Displacement feedback with negative control gains stabilized the flutter mode but caused static divergence to occur. In the Padé model, this phenomenon was predicted in the complex s plane by a positive real aerodynamic pole, which was verified by LTRAN2-NLR time-marching response calculations.

Acknowledgments

The authors acknowledge P. M. Goorjian of NASA Ames and NLR for providing the LTRAN2-NLR code.

References

[1]Ballhaus, W. F. and Goorjian, P. M., "Computation of Unsteady Transonic Flows by the Indicial Method," *AIAA Journal*, Vol. 16, Feb. 1978, pp. 117-124.

[2]Ballhaus, W. F. and Goorjian, P. M., "Implicit Finite-Difference Computations of Unsteady Transonic Flows About Airfoils," *AIAA Journal*, Vol. 15, Dec. 1977, pp. 1728-1735.

[3]Rizzetta, D. P., "Time-Dependent Responses of a Two-Dimensional Airfoil in Transonic Flow," *AIAA Journal*, Vol. 17, Jan. 1979, pp. 26-32.

[4]Guruswamy, P. and Yang, T. Y., "Aeroelastic Time Response Analysis of Thin Airfoils by Transonic Code LTRAN2," *Journal of Computers and Fluids,* Vol. 9, Dec. 1981, pp. 409-425 (also AFFDL-TR-79-3077, June 1979).

[5]Borland, C.J. and Rizzetta, D. P., "Nonlinear Transonic Flutter Analysis," *AIAA Journal*, Vol. 20, Nov. 1982, pp. 1606-1615.

[6]Yang, T. Y. and Chen, C. H., "Transonic Flutter and Response Analyses of Two Three-Degree-of-Freedom Airfoils," *Journal of Aircraft,* Vol. 19, Oct. 1982, pp. 875-884 (also AFWAL-TR-81-3103, Aug. 1981).

[7]Yang, T.Y. and Batina, J. T., "Transonic Time-Response Analysis of Three D.O.F. Conventional and Supercritical Airfoils," *Journal of Aircraft,* Vol. 20, Aug. 1983, pp. 703-710.

[8]Houwink, R. and van der Vooren, J., "Results of an Improved Version of LTRAN2 for Computing Unsteady Airloads on Airfoils Oscillating in Transonic Flow," AIAA Paper 79-1553, July 1979.

[9]Isogai, K., "Numerical Study of Transonic Flutter of a Two-Dimensional Airfoil," National Aerospace Laboratory, Tokyo, Rept. NAL TR-617T, 1980.

[10]Edwards, J. W., Bennett, R. M., Whitlow, W. Jr., and Seidel, D. A., "Time-Marching Transonic Flutter Solutions Including Angle-of-Attack Effects," *Journal of Aircraft,* Vol. 20, Nov. 1983, pp. 899-906.

[11]Batina, J. T., "Transonic Aeroelastic Stability and Response of Conventional and Supercritical Airfoils Including Active Controls," Ph.D. Thesis, Purdue University, West Lafayette, Ind., Dec. 1983.

[12]Batina, J. T. and Yang, T. Y., "Application of Transonic Codes to Aeroelastic Modeling of Airfoils Including Active Controls," *Journal of Aircraft,* Vol. 21, Aug. 1984, pp. 623-630.

[13]Edwards, J. W., "Unsteady Aerodynamic Modeling and Active Aeroelastic Control," Stanford University, Stanford, Calif., Rept. SUDAAR 504, Feb. 1977.

[14]Edwards, J. W., Breakwell, J. V., and Bryson, A. E., "Active Flutter Control Using Generalized Unsteady Aerodynamic Theory," *Journal of Guidance and Control,* Vol. 1, Jan.-Feb. 1978, pp. 32-40.

[15]Noble, B. and Daniel, J. W., *Applied Linear Algebra,* Prentice-Hall, Inc., Englewood Cliffs, N.J., 1977, Chap. 10.

[16]Edwards, J. W., Ashley, H., and Breakwell, J. V., "Unsteady Aerodynamic Modeling for Arbitrary Motions," *AIAA Journal*, Vol. 17, April 1979, pp. 365-374.

[17]Bennett, R. M. and Desmarais, R. N., "Curve Fitting of Aeroelastic Transient Response Data with Exponential Functions in Flutter Testing Techniques," NASA SP-415, 1975, pp. 43-58.

[18]Bucciantini, G., Oggiano, M. S., and Onorato, M., "Supercritical Airfoil MBB A-3 Surface Pressure Distributions, Wake and Boundary Condition Measurements," AGARD-AR-138, May 1979, pp. A8-1—A8-25.

[19]Hassig, H. J., "An Approximate True Damping Solution of the Flutter Equation by Determinant Iteration," *Journal of Aircraft,* Vol. 8, Nov. 1971.

[20]Batina, J. T. and Yang, T. Y., "Transonic Calculation of Airfoil Stability and Response with Active Controls," AIAA Paper 84-0873, May 1984 (also NASA TM-85770, March 1984).